The Astronomical Journal, 130:1278–1285, 2005 September

LIKELIHOOD-BASED METHOD FOR DETECTING FAINT MOVING OBJECTS

Noriaki Miura and Kazuyuki Itagaki[1]
Department of Computer Sciences, Kitami Institute of Technology, 165 Koen-cho, Kitami 090-8507, Japan; miura@cs.kitami-it.ac.jp

and

Naoshi Baba
Department of Applied Physics, Graduate School of Engineering, Hokkaido University, N13W8, Sapporo 060-8628, Japan
Received 2005 January 21; accepted 2005 May 16

ABSTRACT

We present a novel method of detecting faint moving objects in the solar system. The method is based on the evaluation of relative likelihood, which is newly introduced in this paper. Features of this method are that no thresholding operation is required and that both spatial and temporal statistical processing is implemented. These features are advantageous for detecting faint objects. In addition, relative likelihood can be used to quantitatively assess the certainty of detected objects. We applied our method to data taken at two different observatories in Japan. Experimental results indicate that this method is capable of detecting faint moving objects with signals comparable to the noise level.

Key words: methods: data analysis — minor planets, asteroids — techniques: image processing

1. INTRODUCTION

In recent years, the detection of faint moving objects, such as Edgeworth–Kuiper Belt objects (EKBOs) and near-Earth objects, has received much attention. Various image processing techniques for detecting such objects have been proposed and used. We categorize them into two types: statistical and nonstatistical methods.

Methods without statistical processing are straightforward and easily implemented. Levison & Duncan (1990) searched for EKBOs using an image processing method. Rabinowitz (1991) used his moving object detection program in the Spacewatch project. Irwin et al. (1995) described a method using difference maps of images in temporal sequence. Trujillo & Jewitt (1998) presented an image processing method using a circular aperture. Rousselot et al. (1999) developed an algorithm applicable to the detection of trans-Neptunian objects (TNOs).

On the other hand, statistical processing through the use of many frames is an effective way of detecting faint objects. Cochran et al. (1995) described the application of a shift-and-add method to data observed with the *Hubble Space Telescope*. In their method, they subtracted the median sum of all frames from each frame to eliminate stationary objects and then shift-and-added the subtracted images. Gladman et al. (1998) used both shift-and-add and shift-and-median procedures to detect TNOs from data observed from the ground. However, they did not use a refinement procedure as adopted by Cochran et al., because perfect refinement is difficult when the profiles of objects temporarily change as a result of seeing variation. Chiang & Brown (1999) mixed these two methods and modified the refinement procedure. Because a shift-and-add procedure uses tens of frames, these three methods are all capable of detecting very faint moving objects.

Toward further improvement of detection performance are the following three aspects:

1. In the methods without shift-and-add, a kind of thresholding is commonly used to distinguish objects from the sky background. Thresholding is a key factor in specifying the limiting magnitude of a method because it causes faint object candidates to be omitted. We are sure that the limiting magnitude can be improved if no thresholding operation is used in the detection procedure.
2. In shift-and-add-based methods, the removal of stationary objects, such as bright stars, is necessary. If this is not perfectly accomplished, residual objects will hamper the detection of faint moving objects. The procedure of refining frames is therefore a major problem. We think that a method that does not require a refinement procedure could be advantageous.
3. For any detection methods, a theoretical relation between the detection of a moving object and its evaluation should be established. In many conventional methods, the evaluation is usually done with visual inspection after the detection process. We know that such a visual test is very reliable. However, if a visual test is done only for detected objects, there is no guarantee that all the objects will be detected. We believe that detection should be done based on a numerical criterion, namely, quantitatively, and that a detection method has to be capable of detecting all the objects whose evaluation is high enough.

In this paper we propose a novel method that is capable of detecting faint moving objects. Faint objects comparable to sky background are severely affected by photon noise and hence are hardly detected. We therefore introduce a probabilistic interpretation of pixel values and define likelihood on the basis of the Poisson statistical model for photon detection. In our definition of likelihood, statistical processing is done both over the extent of an object and over several images with different observational times. Our method ultimately produces a two-dimensional distribution of likelihood, referred to as a likelihood image. Candidate moving objects are obtained through finding the positions of local maxima in the likelihood image. It should be emphasized that no thresholding operation is employed in the procedure.

2. METHOD

Section 2.1 reviews photon detection under the assumption of a Poisson process and describes the relation between a prior probability specifying a detection process and a posterior

[1] Current address: Image Software Technology Center, Fuji Photo Film Company, 798 Miyanodai, Kaisei-Machi 258-8538, Japan.

probability to be used in the calculation of likelihood. In § 2.2 we model the intensity distribution of a moving object by specifying its parameters of position, velocity, and magnitude. Using the modeled and observed intensity distributions, we define the likelihood of finding consistency between the two distributions. We extend this definition to temporal series images in § 2.3 and then define relative likelihood in § 2.4. The two-dimensional distribution of relative likelihood is used for the detection of moving objects.

2.1. *Photon Detection*

As is widely known, photons striking a detector obey a Poisson stochastic process (Goodman 1985); when incident light has intensity $r(x, y)$ at a position (x, y) on a detector, the conditional probability that intensity $o(x, y)$ will be observed is given by

$$P[o(x,\ y)|r(x,\ y)] = \frac{[r(x,\ y)]^{o(x,\,y)}}{[o(x,\ y)]!}\ \exp[-r(x,\ y)]. \quad (1)$$

Our objective is to find the parameters giving the most probable distribution of $r(x, y)$ according to an observed distribution $o(x, y)$. Thus, we must calculate the posterior probability, $P[r(x, y)|o(x, y)]$, which is the probability that the intensity of incident light is $r(x, y)$ when $o(x, y)$ is observed. Using Bayes's rule, it is given by

$$P[r(x,\ y)|o(x,\ y)] = \frac{P[o(x,\ y)|r(x,\ y)]P[r(x,\ y)]}{\sum_r P[o(x,\ y)|r(x,\ y)]P[r(x,\ y)]}, \quad (2)$$

where the summation is taken over the value range of $r(x, y)$. The term $P[r(x, y)]$ is the probability that light incident to the detector has intensity $r(x, y)$ at a position (x, y). We assume $P[r(x, y)]$ to be constant over the range of $r(x, y)$, because various objects with any brightness, such as stars, moving objects, and sky background, can exist at the position (x, y). This assumption leads to

$$P[r(x,\ y)|o(x,\ y)] = \frac{P[o(x,\ y)|r(x,\ y)]}{\sum_r P[o(x,\ y)|r(x,\ y)]}. \quad (3)$$

Moving objects to be detected are not bright, and their images have a relatively small value of $r(x, y)$. When the range of the summation is wide enough, the denominator nearly equals unity except for when the value of $o(x, y)$ is close to the upper limit of $r(x, y)$. Therefore, we can approximate

$$P[r(x,\ y)|o(x,\ y)] \approx P[o(x,\ y)|r(x,\ y)]. \quad (4)$$

Consequently, we can use equation (1) for the calculation of likelihood.

2.2. *Definition of Likelihood*

We represent the trail of a moving object as $r'_{\boldsymbol{v},\,m}(x, y)$ using parameters of position (x, y), velocity vector $\boldsymbol{v}$, and magnitude m. Figure 1*a* shows an example of $r'_{\boldsymbol{v},\,m}(x, y)$. Next we introduce a point-spread function $h(x, y)$ specifying the extent of the object image caused by diffraction and atmospheric turbulence. In our experiments in § 3, we use a Gaussian function truncated at the radius of its FWHM as $h(x, y)$. The FWHM can be estimated from star profiles in an observed image. We convolve $r'_{\boldsymbol{v},\,m}(x, y)$ with $h(x, y)$ to obtain an intensity distribution under atmospheric turbulence, and then add the sky background, b:

$$r_{\boldsymbol{v},\,m}(x,\ y) = r'_{\boldsymbol{v},\,m}(x,\ y) * h(x,\ y) + b, \quad (5)$$

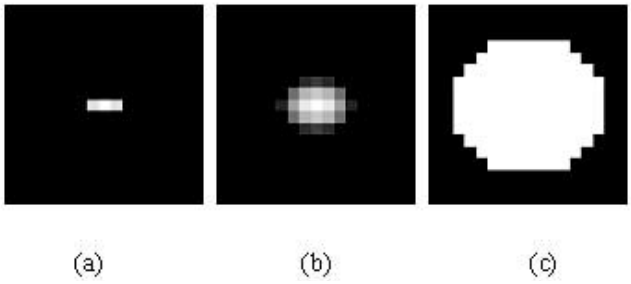

FIG. 1.—Trails of a moving model object (*a*) without blur and (*b*) with blur caused by diffraction and atmospheric turbulence. The white portion in (*c*) specifies the *D*-region inside which the likelihood calculation is carried out. This region is determined by repeating three times an expansion of the image in (*b*) into four neighboring pixels.

where the asterisk denotes a convolution operation. Figure 1*b* shows an example.

Using assumed and observed intensity distributions, we define the logarithmic likelihood of the existence of a moving object with velocity $\boldsymbol{v}$ and magnitude m at a position (x, y):

$$g(x,\ y;\ \boldsymbol{v},\ m) = \ln\left\{\prod_{(x,y)}\prod_{\in D} P\left[r_{\boldsymbol{v},\,m}(x,\ y)|o(x,\ y)\right]\right\} = \sum_{(x,y)}\sum_{\in D} \ln\left\{P\left[r_{\boldsymbol{v},\,m}(x,\ y)|o(x,\ y)\right]\right\}, \quad (6)$$

where D denotes a small region around position (x, y), which should be larger than the extent of the moving object. We specify D by repeating three times an expansion of the moving object image into four neighboring pixels, where we experimentally determine the degree of expansion. The shape of the object intensity distribution becomes almost like an ellipse, as shown in Figure 1*b*. Thus, the shape of D also becomes like an ellipse (Fig. 1*c*).

We calculate $g(x, y; \boldsymbol{v}, m)$ using various values of $\boldsymbol{v}$ and m and then find the maximum value among them. We denote this as the existent likelihood of a moving object at the position (x, y):

$$L'(x,\ y) = \max|_{\boldsymbol{v},\,m}[g(x,\ y;\ \boldsymbol{v},\ m)]. \quad (7)$$

Calculating equation (7) over the image region, we obtain the two-dimensional distribution of existent likelihood.

2.3. *Extension to Temporal Series Images*

Several images are ordinarily observed in the same field of view in a time sequence. We can use them to distinguish moving objects from fixed ones, such as stars and galaxies. We represent observed images as $o_n(x, y)$ $(n = 1, \ldots, N)$, where N is the number of frames. Of course, we know the exposure time and the observation intervals between exposures. Specifying the velocity and the position (x_1, y_1) of a moving object in the first frame, we can derive the expected positions (x_n, y_n) of the moving object in the nth frame. Using this expression, we redefine the existent likelihood at position (x_1, y_1) in the first frame by

$$L(x_1,\ y_1) = \max|_{\boldsymbol{v},m}\left[\sum_{n=1}^{N} g_n(x_n,\ y_n;\ \boldsymbol{v},\ m)\right], \quad (8)$$

where

$$g_n(x_n,\ y_n;\ \boldsymbol{v},\ m) = \sum_{(x_n, y_n)} \sum_{\in D} \ln\{P[r_{\boldsymbol{v}, m}(x_n,\ y_n) | o_n(x_n,\ y_n)]\}. \tag{9}$$

We calculate equation (9) at all positions in the first frame to obtain the two-dimensional distribution of existent likelihood, $L(x, y)$. It should be noted that equations (8) and (9) include statistical processing of temporal and spatial summations, respectively. Thus, we can expect good performance in detecting faint objects.

2.4. *Definition of Relative Likelihood*

In our definition of likelihood, the likelihood is large regardless of m when the magnitude m coincides with $o(x, y)$. Therefore, large likelihood is distributed not only on the positions of moving objects but also over the background, because very faint objects could be supposed to exist at any position in the background. On the other hand, likelihood at the positions of stationary objects becomes smaller. As a consequence, the likelihood distribution $L(x, y)$ will be like the negative of the observed image, and its contrast will be governed by bright stationary stars. From this distribution, it is difficult to directly search for true moving objects. We think that an additional process is necessary to emphasize the likelihood of moving objects compared to their brightness. For this purpose, we introduce the relative likelihood, defined as follows: First, we assume that no object exists at a position (x_n, y_n) in the nth frame. That is, intensity distribution in equation (5) is assumed to be just the sky background. In this case we represent the intensity distribution as $r_{\boldsymbol{v}, \infty}(x, y)$, where the magnitude parameter m is denoted as infinity. Using $r_{\boldsymbol{v}, \infty}(x, y)$, we calculate the nonexistence likelihood $\hat{L}(x_1, y_1)$ at a position (x_1, y_1) in the first frame as

$$\hat{L}(x_1,\ y_1) = \sum_{n=1}^{N} g_n(x_n,\ y_n;\ \boldsymbol{v},\ \infty). \tag{10}$$

Calculating this equation over the image region, we obtain the two-dimensional distribution of nonexistent likelihood, $\hat{L}(x, y)$. Using the existent likelihood $L(x, y)$ and the nonexistent likelihood $\hat{L}(x, y)$, both of which have negative values, the relative likelihood is defined by

$$I(x,\ y) = 1 - \frac{L(x,\ y)}{\hat{L}(x,\ y)}. \tag{11}$$

Here we set its negative values to zero. We call $I(x, y)$ the "likelihood image." If $L(x, y) > \hat{L}(x, y)$, namely, if $|L(x, y)| < |\hat{L}(x, y)|$, then $I(x, y)$ becomes positive. This case indicates that a moving object is likely to exist rather than not to exist. On the other hand, if $L(x, y) \leq \hat{L}(x, y)$, then a moving object probably does not exist. Since we are not interested in the latter case, we force negative values in $I(x, y)$ to be zero. As a result, $I(x, y)$ ranges from zero to unity.

The right-hand side of equation (11) is rewritten as $[L(x, y) - \hat{L}(x, y)]/[-\hat{L}(x, y)]$. Its numerator evaluates the increment of likelihood when assuming the existence of a moving object. The denominator $-\hat{L}(x, y)$ becomes larger for brighter objects, because no object is assumed to exist at the position (x, y). Thus, the division by $-\hat{L}(x, y)$ reduces the effect of bright objects. As can be seen, the relative likelihood $I(x, y)$ is the normalized increment of likelihood. A larger value of $I(x, y)$ indicates a higher possibility of the existence of a moving object. Thus, we can regard a likelihood image $I(x, y)$ as the two-dimensional distribution of probability of whether a moving object exists.

Candidates of moving objects show local peaks with larger values in $I(x, y)$. We detect them through finding peaks in order of their values. An advantage of our method is that the values of $I(x, y)$ are useful for observers to assess the certainty of detected objects.

3. EXPERIMENTS

We apply our method to two data sets obtained with different observational conditions. To assess the experimental results in spite of different observational conditions, we compare the average brightness of detected objects with the noise level. We regard the performance of a method as better when the mean brightness of detected objects is closer to the noise level. As is usually done, we take the noise level σ as the standard deviation around the sky background b over a region that contains no stars. As the mean brightness, we use the average excess of pixel intensities above the sky background inside the extent of the moving object.

In the calculation of equation (8), we have to survey parameters $\boldsymbol{v}$ and m. To specify the velocity $\boldsymbol{v}$, we use two quantities, the speed $u = |\boldsymbol{v}|$ and its direction θ, which is the counterclockwise angle from the x-axis. As a result, the parameters to be surveyed are u, θ, and m. We denote the step widths of these parameters as Δu, $\Delta\theta$, and Δm, respectively.

3.1. *Experiment I*

We observed known main-belt asteroids with the 115 cm telescope of the Rikubetsu Astronomical Observatory in Japan. The observational time was 16:53:00 on 2001 September 21 (UT). A cooled CCD camera was used for detection. The exposure time was 5 minutes, and the interval between exposures was 10 minutes. The average FWHM of star profiles was about 2.″9. Figure 2 shows the observed images, gamma-corrected to emphasize dark parts. These images have 8 bit gray levels and 512×512 pixels, which corresponds to $3.'28 \times 3.'28$. As can been seen, the signal-to-noise ratios of the images were not so good because the cooling of the CCD camera was not enough. We also observed standard stars for calibration soon after the asteroid observation.

The images used in this experiment contain two known main-belt asteroids, Gigli and 2001 XZ73. Their estimated magnitudes are 20.5 and 19.8, respectively. Subimages in Figure 2 display regions around the asteroids. We hardly recognize the asteroids because of severe noise. Figure 3 plots the mean brightness of the asteroids and the noise level. Some values of the mean brightness are lower than the noise level. If thresholding were applied to this image, the detection of the asteroids would have failed.

We calculated the relative likelihood over the image region with the following parameter ranges and scan intervals: $m = 18.0-22.0$ and $\Delta m = 0.5$; $u = 0.''2-0.''5$ minute^{-1} and $\Delta u = 0.''05$ minute^{-1}; $\theta = 0^\circ-359^\circ$ and $\Delta\theta = 1^\circ$. Figure 4 shows the resulting likelihood image. The subimages display the same regions as in Figure 2. We find peaks of relative likelihood at the positions where asteroids are expected to be. However, there are many peaks that are not only asteroids but also noise. Table 1 shows the relative likelihood values of large peaks in order. The peaks in the first and second rows arise from asteroids, and their values notably exceed those of noise peaks. Consequently, we succeeded in detection of the asteroids whose brightness was comparable to the noise level. The limiting magnitude of

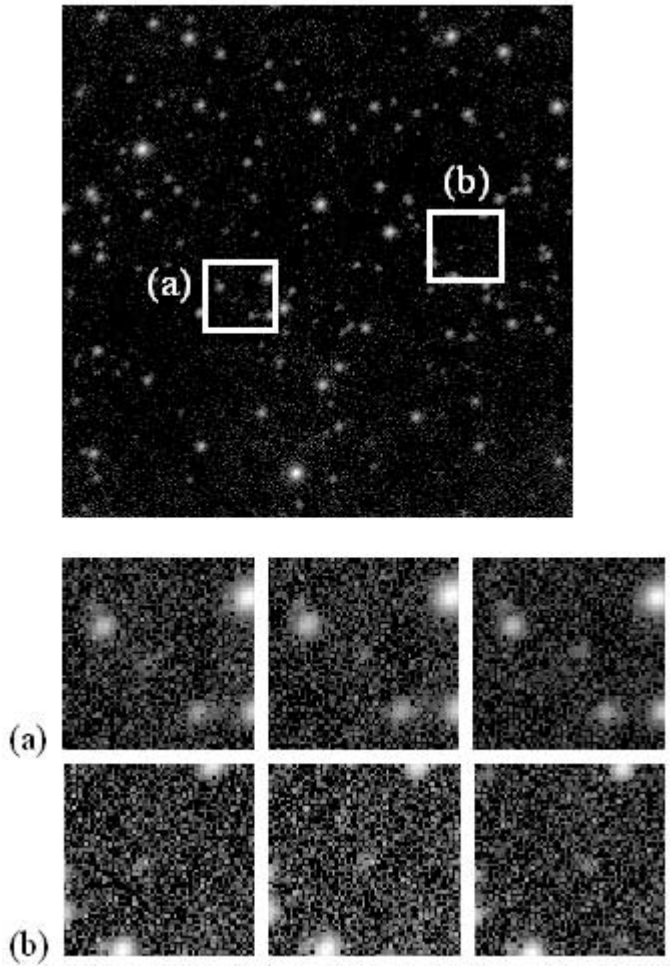

FIG. 2.—*Top*: One of the images observed at the Rikubetsu Observatory. The squares indicate the regions where asteroids exist. The images in the middle and bottom rows show the temporal sequences of the asteroids 2001 XZ73 and Gigli, respectively, corresponding to the regions *a* and *b*.

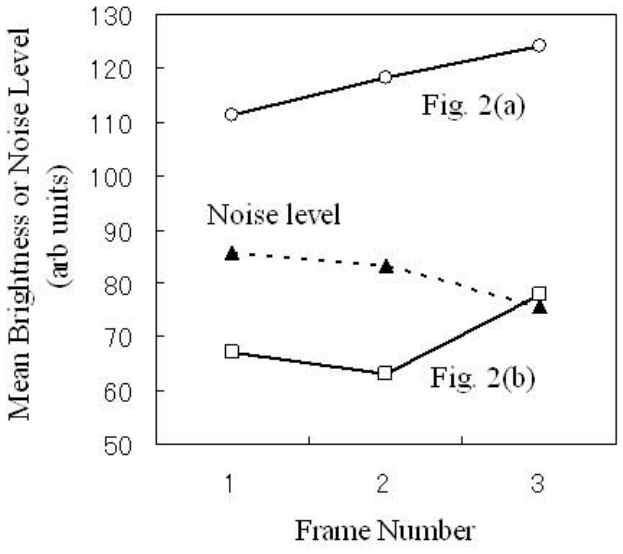

FIG. 3.—Mean brightness (*circles and squares*) compared with noise level (*triangles*). Two values of the mean brightness are lower than the noise level.

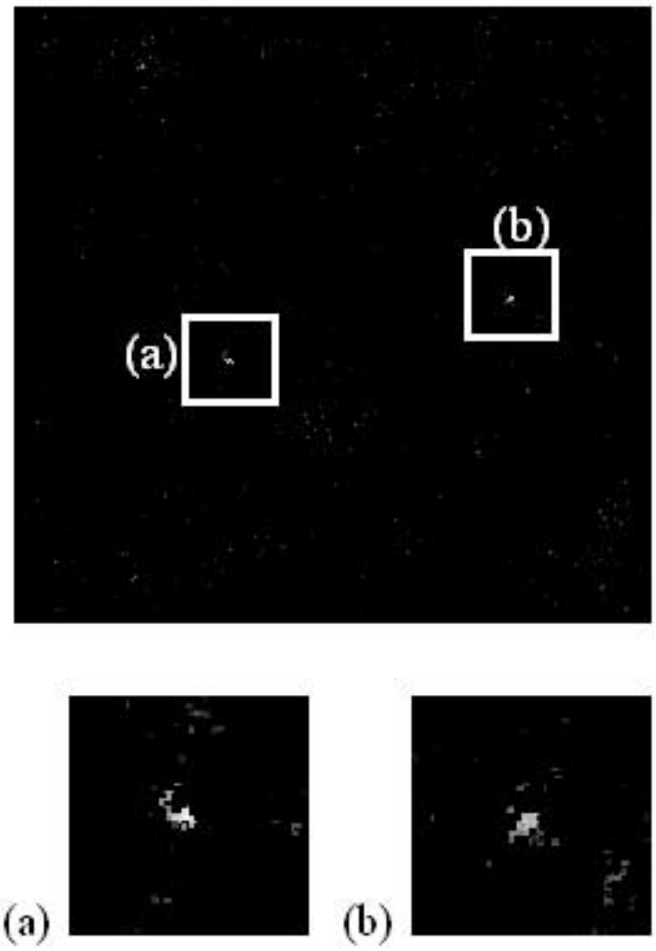

FIG. 4.—*Top*: Two-dimensional distribution of the resulting likelihood. *Bottom*: Regions around the asteroids, which correspond to regions *a* and *b* in Fig. 2. Large peaks appear at the centers of these images.

this observation can be larger than 20 because the value of relative likelihood in the second row (asteroid of 20th magnitude) has notable excess compared with that in the third row (noise of 20th magnitude).

3.2. *Experiment II*

The images used in this experiment were taken with a cooled CCD camera on the 25 cm telescope at the Bisei Space Guard Center in Japan. The observation was done at 15:24:23 on 2001 January 17 (UT). The exposure time and interval between exposures were 2.5 and 15 minutes, respectively. The images are

TABLE 1
DETECTED PEAKS OF RELATIVE LIKELIHOOD IN ORDER AND THEIR PARAMETERS FROM EXPERIMENT I

		PARAMETERS				
ORDER	$I(x, y)$	x	y	u	θ	m
1.....	0.4736	174	293	0.20	320	19.5
2.....	0.3701	399	242	0.35	356	20.0
3.....	0.2680	373	369	0.25	225	20.0
4.....	0.2654	19	345	0.20	138	20.0
5.....	0.2553	198	454	0.45	287	20.5

NOTE.—Two asteroids, 2001 XZ73 and Gigli, are ranked first and second, respectively.

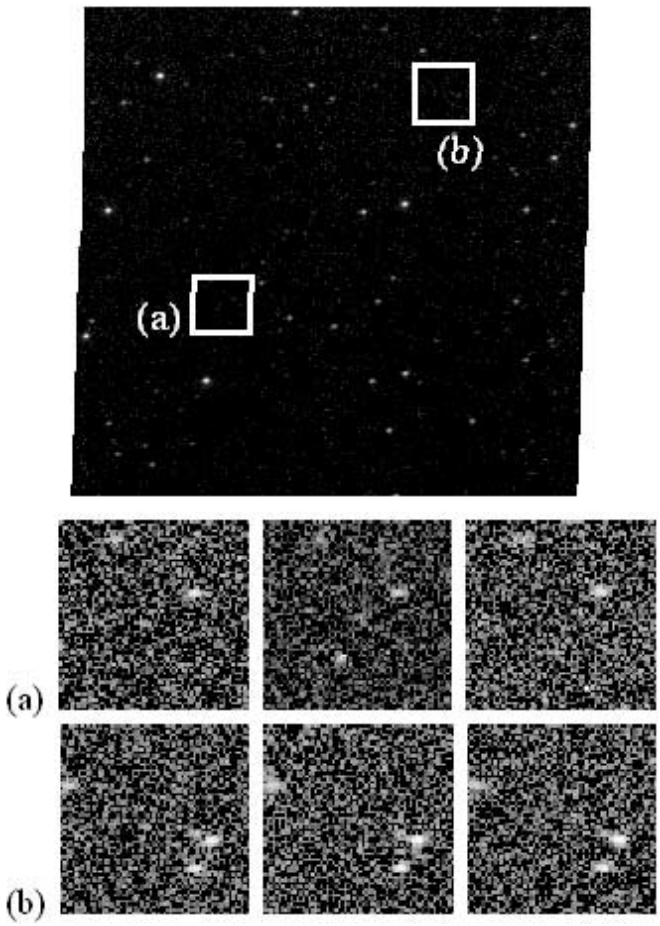

FIG. 5.—*Top*: One of the images observed at the Bisei Space Guard Center. The squares indicate the regions where asteroids exist. The images in the middle and bottom rows show the temporal sequences of the asteroids 1999 TA141 and 2000 YC116, respectively, corresponding to regions *a* and *b*.

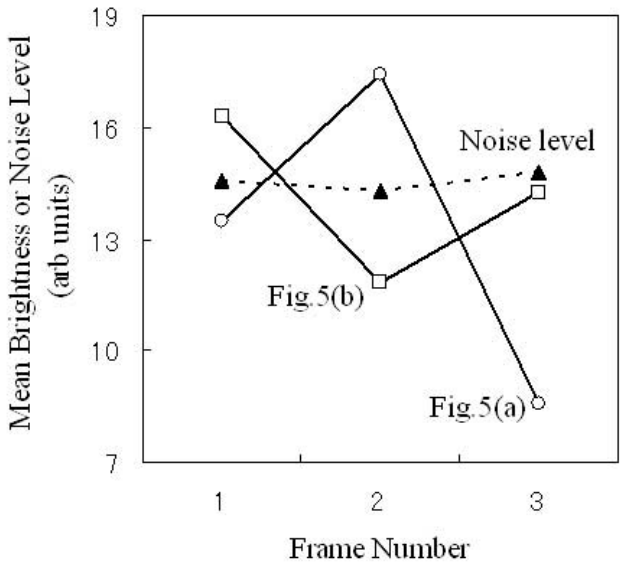

FIG. 6.—Mean brightness (*circles and squares*) compared with noise level (*triangles*). Two values of mean brightness are lower than the noise level in each case of *a* and *b*.

shown in Figure 5 and have been gamma-corrected. The image size is 512×512 pixels, which corresponds to $19.'5\times19.'5$. In these images, two known main-belt asteroids, 1999 TA141 and 2000 YC116, exist. Their estimated magnitudes are 18.6 and 18.9, respectively. The subimages within squares *a* and *b* in Figure 5 show the regions featuring the respective asteroids. Unfortunately, we have no calibration data for this set of images. Thus, we calibrated the magnitude values in accordance with the relation between the intensity values of detected asteroids and their estimated magnitude.

Figure 6 plots the average brightness and noise level. As can been seen, several values of mean brightness are under the noise level. The detection of these asteroids would have been difficult if a thresholding process had been applied.

Parameter ranges and intervals in this experiment were $m = 16.0–21.0$ and $\Delta m = 0.5$; $u = 0.''5–0.''8$ minute^{-1} and $\Delta u = 0.''05$ minute^{-1}; $\theta = 0^\circ–359^\circ$ and $\Delta\theta = 1^\circ$. Figure 7 shows the likelihood image obtained with these parameters. In the subimages we see large peaks of relative likelihood. Table 2 lists the detected peaks in order. The values of relative likelihood corresponding to known asteroids are in the top two rows. This indicates that our method is capable of detecting a faint asteroid that is hardly distinguishable from noise. However, the likelihood value of the second row is very close to the third one. The third one is not a main-belt asteroid because the direction differs significantly from those of the top two. More observations are necessary to judge whether it is a real moving object. Accordingly, if

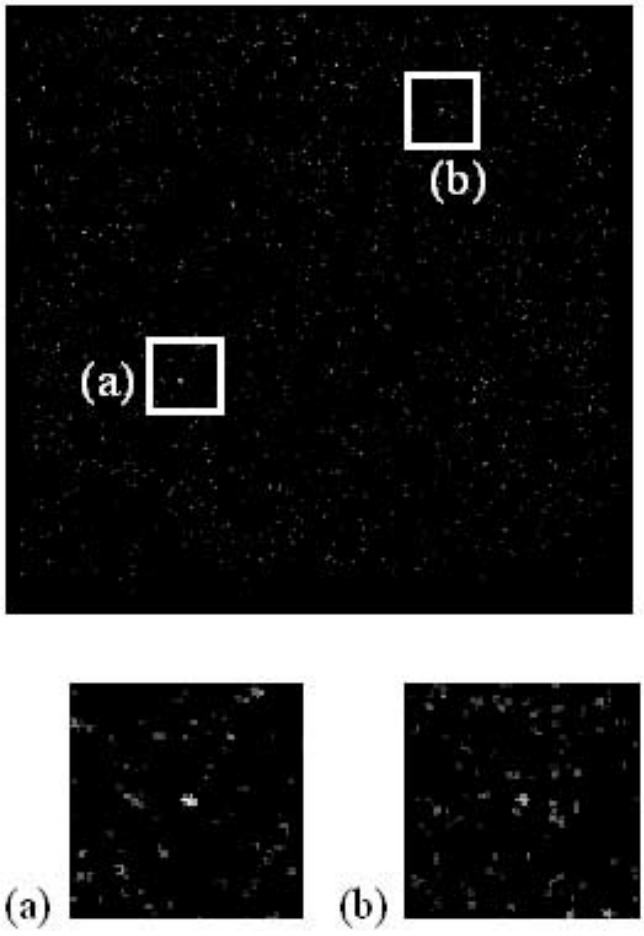

FIG. 7.—*Top*: Two-dimensional distribution of the resulting likelihood. *Bottom*: Regions around the asteroids, which correspond to regions *a* and *b* in Fig. 2. Large peaks appear at the centers of these images.

TABLE 2
DETECTED PEAKS OF RELATIVE LIKELIHOOD IN ORDER AND THEIR PARAMETERS FROM EXPERIMENT II

		Parameters				
Order	$I(x, y)$	x	y	u	θ	m
1.....	0.3176	141	315	0.70	336	18.5
2.....	0.2320	355	88	0.55	329	19.0
3.....	0.2242	382	333	0.75	55	19.0
4.....	0.2235	54	233	0.55	214	18.5
5.....	0.2197	215	404	0.80	329	19.0

NOTE.—Two asteroids, 1999 TA141 and 2000 YC116, are ranked first and second, respectively.

we did not have a priori information on these objects, we could not be perfectly confident that the second peak arose from a real object. Nevertheless, we have succeeded in detecting an asteroid of 19th magnitude from images observed with a 25 cm telescope. The limiting magnitude would become larger if we used a larger telescope.

4. DISCUSSION

4.1. *Effect of Increasing the Number of Frames*

The number of data frames is a free parameter in our method. Thus, we must investigate how many frames are necessary for successful detection. The data set used here is same as in experiment II. Changing the number of frames, we calculated the relative likelihood in order to obtain likelihood images. Figures 8*a*–8*d* show the likelihood images obtained from one, two, three, and four frames, respectively. The central part of these images is the same as region *b* in Figure 5. Comparing Figure 8*a* with region *b* in Figure 5, we find that the influence of stars was not removed when only one frame was used. In the likelihood image obtained from two frames, the influence of stars disappears. However, asteroids could not be detected because the values of relative likelihood at asteroid positions were not larger than those at the other positions. When the number of frames was three, we succeeded in the detection, as described in § 3.2. As the number of frames increased, noise peaks were suppressed, as shown in Figure 8*d*. In summary, the use of three frames is mandatory for obtaining a successful result, and more frames will provide better results. This may not be novel information for observers who use other detection methods, because the use of three frames is common in such methods. However, one can visually understand the effect of increasing the number of frames in Figure 8.

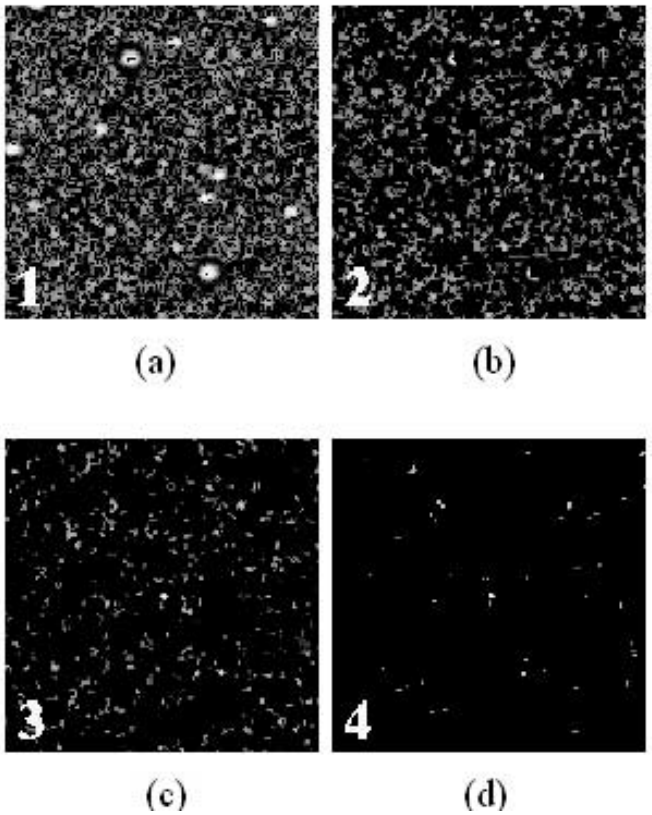

FIG. 8.—Likelihood images demonstrating the effect of increasing the number of frames. They display region *b* in Fig. 5. The numbers inside the images are the number of frames used in the likelihood calculation. As the number of frames increases, peaks from noise are suppressed, and the peak from the asteroid becomes more noticeable.

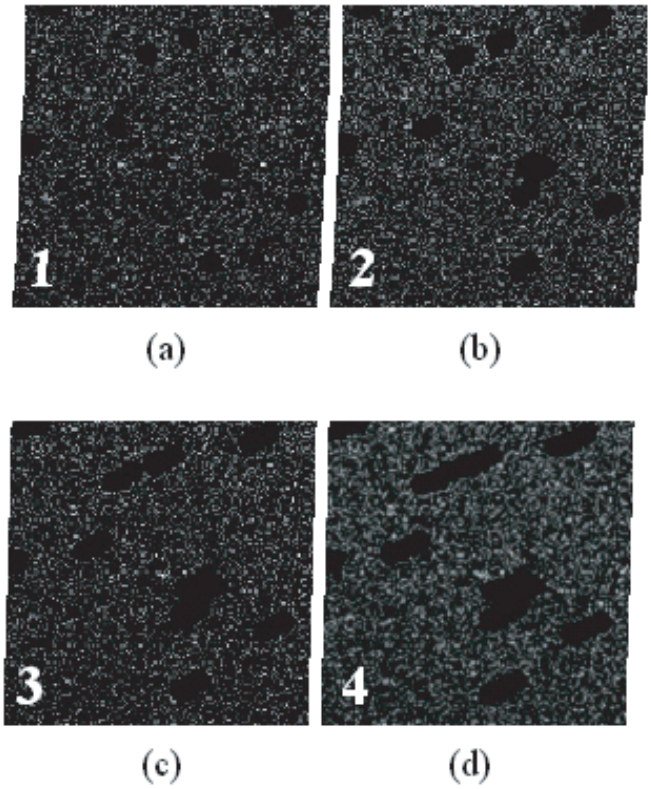

FIG. 9.—Results of shift-and-add using (*a*) one, (*b*) two, (*c*) three, and (*d*) four frames. The same data set as used in Fig. 8 was processed. The label indicates the number of summed frames. An asteroid appears at the image center and becomes more distinct as the number of frames increases.

4.2. *Comparison with Shift-and-Add*

Compared with the shift-and-add-based methods (Cochran et al. 1995; Gladman et al. 1998; Chiang & Brown 1999), our method is somewhat complex to implement and will require more computational time. Here we compare the performance of our method with shift-and-add with the data set used for Figure 8.

First, we masked stars brighter than the asteroid that exists in the observed images (see Fig. 9*a*). Using the velocity $\boldsymbol{v}$ determined with our method, we shifted images so that the asteroid appeared at the center in all frames and then added the shifted images to the first frame one by one. Figures 9*a*–9*d* show the results of shift-and-add using one, two, three, and four frames,

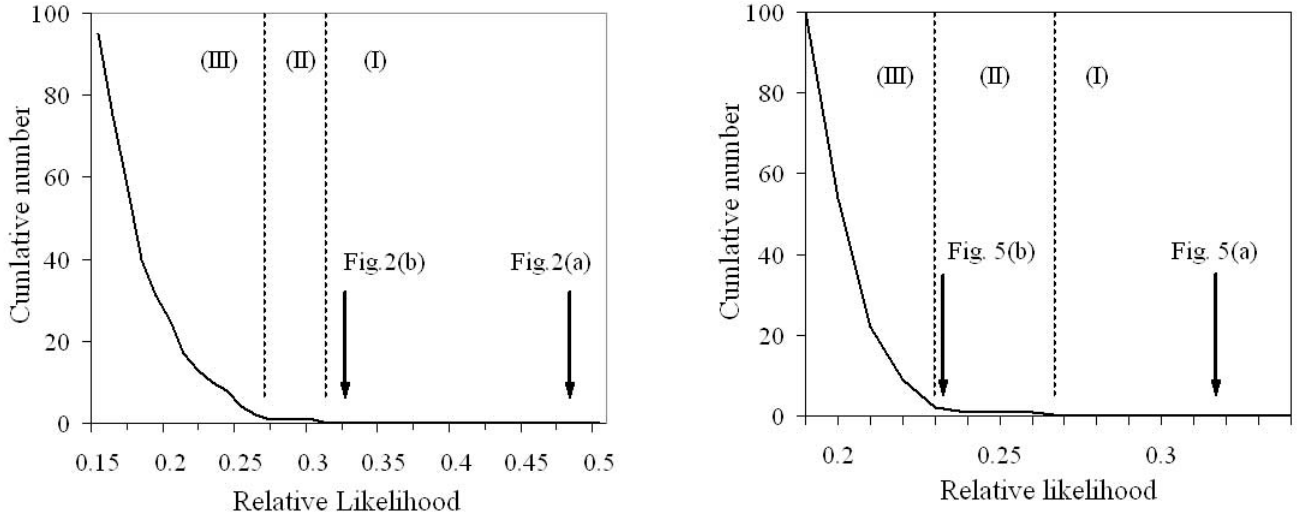

FIG. 10.—Total number of noise peaks with values larger than the relative likelihood specified in the horizontal axis, for experiment I (*left*) and experiment II (*right*). The arrows point to the relative likelihood of the true asteroids, which are listed in Tables 1 and 2. The labels I, II, and III show three specific sections of relative likelihood: candidates detected in sections I, II, and III are regarded as certainly real, probably real, and certainly false, respectively. Three of the four detected objects are in section I. However, one arrow in the right panel lies in section II.

respectively, in the same configuration as Figure 8. As the number of frames increases, the object at the center becomes more noticeable. This demonstrates the effect of frame addition. However, it seems that the distinction of the signal component from surrounding noise is not easier than in Figure 8. To numerically confirm that, we calculated the contrast of the signal as (signal − mean)/noise, where "signal" is the value at the image center, "mean" is the average of pixel values, and "noise" is the standard deviation of the surrounding noise. The resulting values of Figures 9*a*–9*d* are 2.77, 4.05, 6.68, and 5.64, respectively, while those of Figures 8*a*–8*d* are 2.17, 2.76, 6.94, and 12.4. The low contrast in Figure 9*d* is due to the bad seeing conditions in the fourth frame.

From these results, we conclude that the detection of objects in likelihood images is easier than in shift-and-add images. This is because statistical processing is done only temporally in the shift-and-add, while it is done both temporally and spatially in the calculation of likelihood.

4.3. *Estimation of True or False Detection*

In order to determine whether detected objects are real, we should know how noise alignments are evaluated in terms of relative likelihood. For this purpose, we conducted the following experiments: we changed the order of frames in use to 1, 3, 2 and 2, 1, 3 and then carried out the detection procedure for each order. Of course, any true objects would never be detected. That is, all the peaks in likelihood images arise from noise alignments. In the two resulting likelihood images, we counted the numbers of peaks larger than a specified relative likelihood and then summed them.

The plots in Figure 10 (*left*, *right*) show the summed number of peaks when changing the specified relative likelihood for experiments I and II, respectively. One finds that the two graphs have nearly the same profiles, but their horizontal positions are different. This indicates that the absolute values of relative likelihood differ with observational conditions. In Figure 10 (*left*) the maximum relative likelihood of noise alignment is 0.3060. Compared with this, 0.4736 and 0.3710, which are the relative likelihoods of true objects, are significantly large. In Figure 10 (*right*) the relative likelihood of one asteroid, 0.3176, is larger than the maximum value of the noise peaks, 0.2642. In this case we can judge that this asteroid is real. However, for the other asteroid, its relative likelihood, 0.2320, is smaller than those of some noise peaks.

The axis of relative likelihood can be divided into three specific sections: (I) there is no noise peak; (II) the profiles are nearly flat; and (III) the profiles are descending. We regard objects with values in sections I or III to be certainly real or certainly false. In section II noise peaks exist but are rare events. The peaks in section II have a relatively high probability of being real and thus should be further investigated.

It should be noted again that the profiles of relative likelihood depend on observational conditions. Thus, to specify sections I–III, users must repeat observations in their own conditions. However, once the sections are determined for one observational condition, they will be used for another observation whose conditions are the same.

4.4. *Computational Time*

Calculation of equation (8) over the whole image region takes much computational time, because the algorithm requires octuple loops with respect to position, extent, speed, direction, magnitude, and the number of frames. For example, the computational time was 210 s in experiment II using a standard PC with a Pentium IV 2.8 GHz processor. If three 2048×4096 images were used, then the computational time would have been 112 minutes. We think that a feasible method must complete the calculation within the time spent in acquiring a set of data. If this were realized, users could obtain detection results during the observation of the next target. In experiments I and II, it took 35 and 37.5 minutes for the observations, respectively. Thus, if the computational time could be shortened by a factor of 4, our method would be useful in a practical situation. This would be valid when using more than three frames, because observational time also increases with the number of frames.

To reduce computational time, we can widen the scan intervals of the parameters. Through experiments, we confirmed that detection was successful when $\Delta\theta < 10^\circ$. For example, setting $\Delta\theta = 4^\circ$ reduces computational time to a quarter of the

original. A good technique is to first apply a relatively wide interval over the whole range and then to reapply a narrow interval only over the range in which an object would exist.

For some objects, such as main-belt asteroids and EKBOs, the ranges of direction and speed to be surveyed can be greatly reduced because their directions and speeds do not deviate much from the average. If we restrict the direction range to 90°, this reduces computational time by one-fourth.

Another feasible idea is to simultaneously use our method to detect faint objects and another fast method for brighter ones. In this case we can restrict the magnitude parameter m of our method to be over only a dark range, for example, beyond 20th magnitude.

Using better hardware is a simple and straightforward solution. For example, by simply using a PC with dual processors, half of the computational time is saved. Recently, mosaic CCD cameras with 10 2048×4096 chips became available in some observatories, such as the Subaru telescope and the Bisei Space Guard Center. To process data from such cameras, the use of a PC cluster is reasonable. By separately processing images from each chip with each PC in the PC cluster, the increase of computational time will be suppressed.

5. CONCLUSION

We presented a novel method of detecting astronomical moving objects. The method contains statistical processing of both spatial and temporal averaging and ultimately results in a two-dimensional distribution of relative likelihood (likelihood image). In this paper, for the first time, to our knowledge, relative likelihood has been defined. We can detect moving objects through finding large local peaks in the likelihood image. Features of our method are as follows:

1. No thresholding is applied.
2. No refinement procedure of removing stationary objects is required.
3. The value of relative likelihood is useful for assessing the certainty of the detected candidates.
4. Statistical processing is done both spatially and temporally.
5. Candidates with large values of relative likelihood are detected in order.

We applied our method to images taken at the Rikubetsu Observatory and at the Bisei Space Guard Center in Japan. From the experiments, we found the following:

1. Our method can detect asteroids at more than 20 mag using a 115 cm telescope.
2. Our method is capable of detecting an asteroid at about 19.5 mag with a 25 cm telescope.
3. To successfully implement our method, three frames are necessary, and more frames leads to better results.
4. Detection of candidates in likelihood images is easier than in shift-and-add images.

From these results, we conclude that our method is effective in detecting faint objects with signals comparable to the noise level. Although our method consumes large computational time, we pointed out that computational time can be easily reduced and that our method will be useful in practical situations.

We especially thank Y. Yamashita, the director of the Rikubetsu Observatory, for his help during our observations and for valuable advice. We also thank the staff of the Rikubetsu Observatory for their assistance. We thank M. Yoshikawa and S. Isobe for providing us the data observed at the Bisei Space Guard Center. N. M. thanks M. Nagahara for his assistance in experiments.

REFERENCES

Chiang, E. I., & Brown, M. E. 1999, AJ, 118, 1411
Cochran, A. L., Levison, H. F., Stern, S. A., & Duncan, M. J. 1995, ApJ, 455, 342
Gladman, B., Kavelaars, J. J., Nicholson, P. D., Loredo, T. J., & Burns, J. A. 1998, AJ, 116, 2042
Goodman, J. W. 1985, Statistical Optics (New York: Wiley)
Irwin, M., Tremaine, S., & Zytkow, A. N. 1995, AJ, 110, 3082
Levison, H. F., & Duncan, M. J. 1990, AJ, 100, 1669
Rabinowitz, D. L. 1991, AJ, 101, 1518
Rousselot, P., Lombard, F., & Moreels, G. 1999, A&A, 348, 1035
Trujillo, C., & Jewitt, D. 1998, AJ, 115, 1680